Inorganic Chemistry

pubs.acs.org/IC Article

Boosting Selective Adsorption of Xe over Kr by Double-Accessible Open-Metal Site in Metal−Organic Framework: Experimental and Theoretical Research

Yuan Tao, Yaling Fan, Zhenzhen Xu, Xuefeng Feng, Rajamani Krishna, and Feng Luo*

Cite This: *Inorg. Chem.* 2020, 59, 11793−11800 Read Online

ABSTRACT: Obtaining highly valuable Xe from air or other sources is highly important but still seriously restricted by its inherent inert nature and the great difficulty in separation from other inert gases, especially for Xe and Kr that show comparable size. In this work, we show both experimental and theoretical research of how to boost the selective adsorption of Xe over Kr by double-accessible open-metal site in metal−organic framework (MOF). The MOF, namely, UTSA-74, shows a high Xe uptake up to 2.7 mmol/g and a lower Kr uptake of 0.58 mmol/g at 298 K and 1 bar, leading to a high selectivity of 8.4. The effective Xe/Kr separation was further confirmed by both transient breakthrough simulation and experimental breakthrough. The separation mechanism, as unveiled by the grand canonical Monte Carlo simulation and dispersion-corrected density functional theory calculation, is due to the unique double-accessible open-metal site in UTSA-74 that affords stronger interaction toward Xe than Kr.

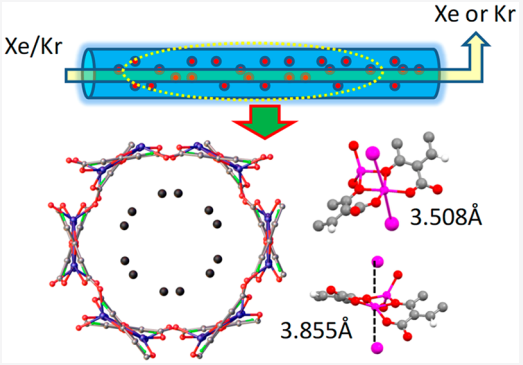

INTRODUCTION

Since the first discovery of Kr and Xe in the late 19th century, these species have received extensive attention, due to their great and broad applications in medical imaging, commercial lighting, insulation, lasers, illumination, and spacecraft propellants.[1−4] They can be generally obtained as a byproduct from air separations with a 20:80 (v/v) Xe/Kr mixture. Alternatively, Xe and Kr can be obtained from the off-gas of nuclear fuel (UNF).[5−7] Currently, the mature technique to generate such products is based on their different boiling points via cryogenic distillation, however, which presents an energy- and cost-intensive avenue.

Adsorption-based separation upon porous solid materials presents a low-cost and low-energy alternative.[8] Accordingly, the traditional solid porous materials such as porous carbon and zeolites have been extensively investigated for Xe/Kr separation, however, just showing low adsorption capacity and selectivity, seriously restricting their practical applications.[9−11] This is mainly because Xe and Kr show inert physical and chemical properties and the same shape and close diameters (Xe, 4.1 Å vs Kr, 3.7 Å).

In the past decades metal−organic frameworks (MOFs) have been witnessed to show big potential in gas separation, including in alkyne/alkene, alkene/alkane, isomer, and isotope counterpart.[12−19] However, only limited MOFs have been researched for such task, mainly because of their inherent inert nature that consequently leads to weak interaction with the skeleton of MOFs and the serious requirement for the size effect.[20−34] In this regard, some benchmark work and theoretical research discloses that MOFs with the pore size of ∼4.0 Å benefit the enhancement of the Xe adsorption selectivity. For example, Li et al. reported an MOF with pore size of (4.1 Å × 4.3 Å), showing ultrahigh Xe selectivity up to 60.6 at the low pressure of 0.2 bar.[33] Xing et al. designed a narrow pore with size of ∼3.3 Å but local flexibility, leading to the recorded Xe/Kr uptake ratio up to 43 at 0.2 bar and 273 K.[34] SBMOF-1 created by Thallapally et al. enables a 4.2 Å pore size, well matching with a Xe atom, resulting in a thermodynamic Xe/Kr selectivity of 16 at 298 K.[29] All these results indicate that the narrow pore of ∼4.0 Å benefit the restriction of the Xe molecule through weak van der Waals intermolecular interaction, consequently leading to Xe adsorption selectivity, though Xe shows an inherent inert nature. To enhance the intermolecular affinity, an open-metal site in MOFs was approved to be effective toward Xe, lying on the unique metal-Xe contact. For example, Cu-BTC, a typical MOF holding an open Cu site, affords Xe adsorption

Received: June 15, 2020
Published: July 31, 2020

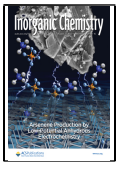

https://dx.doi.org/10.1021/acs.inorgchem.0c01766
Inorg. Chem. 2020, 59, 11793−11800

selectivity of 2.6,[20] while increasing the density of open-metal site such as Ni-MOF-74 with open Ni site leads to higher Xe adsorption selectivity up to 5,[7] though the pore size in both of them is more than 11 Å, far larger than the Xe atom. In this regard, our recently reported UTSA-74[35] that shows higher density of open-metal site than Ni-MOF-74 is expected to render higher Xe adsorption selectivity.

As expected, Xe adsorption selectivity up to 8.4 at room temperature and 1 bar was observed in UTSA-74. And excellent Xe/Kr separation was also reflected on the experimental breakthrough. Grand canonical Monte Carlo (GCMC) simulation discloses that the major adsorption locates on the double open-metal site, while the dispersion-corrected density functional theory (DFT-D) calculation reveals a strong contact between the open Zn site and Xe, showing a shorter distance of 3.5 Å for Zn−Xe than Zn−Kr (3.8 Å).

MATERIALS AND METHODS

Materials and Physical Measurements. The reagents and solvents were commercially available and were used as received without further purification. X-ray powder diffraction (PXRD) patterns were collected by a Bruker AXS D8 Discover powder diffractometer at 40 kV, 40 mA for Cu Kα (λ = 1.5406 Å) at room temperature in the range of 5−50° (2θ) with a scan speed of 0.1 deg per step. The gas sorption isotherms were collected on a Belsorp-max. Ultrahigh-purity-grade (>99.999%) Xe and Kr gases were used in this adsorption measurement. To maintain the experimental temperatures, a temperature-programmed water bath (273 and 298 K, respectively) was used.

Synthesis of UTSA-74. The synthesis of it followed our previous reported method.[35] A dimethyl formamide (DMF) (10 mL)/H_2O (0.5 mL) solution of $Zn(NO_3)_2{\cdot}6H_2O$ (1 mmol) and H_4dobdc (0.5 mmol) was sealed in a Teflon reactor, heated at 150 °C for 3 d, and then cooled to room temperature at 3 °C/h. Subsequently, block crystals were obtained in 82% yield based on Zn. Elemental analysis: Calcd for $Zn_2(H_2O)(dobdc){\cdot}0.5(H_2O)(C_8H_5O_{7.5}Zn_2)$: C, 27.30; H, 1.43; Found: C, 27.13; H, 1.40. The active method for UTSA-74 refers to our previous report. The as-synthesized samples were immerged in CH_3OH for 3 d with the replacement of fresh CH_3OH three times per 1 d. Then the samples were first degassed under vacuum to get dry samples. Later, the samples were further degassed under vacuum at 200 °C for 24 h on Belsorp-max. The samples were confirmed by powder X-ray diffraction (Figure 1).

Breakthrough Experiment. The experimental setup used for dynamic measurements is homemade. Before performing the breakthrough experiment, 1.5 g of the activated adsorbent (in the column Ø 6 mm × 300 mm) was activated at 200 °C overnight under vacuum. Before starting each experiment, helium reference gas is flushed through the column, and then the gas flow is switched to the desired gas mixture at the same flow rate of 2 mL/min. The gas mixture downstream the column was monitored using a Hiden mass spectrometer. The recycle breakthrough experiment was performed in such way when the samples finished the breakthrough experiment; then, the samples were activated at 100 °C under vacuum for 2 h, and later the next breakthrough experiment was performed.

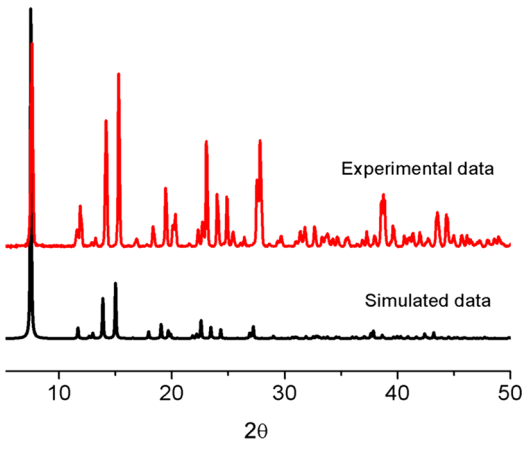

Figure 1. Experimental PXRD pattern of as-synthesized UTSA-74 samples and simulated from the single-crystal data.

Fitting of Experimental Data on Pure Component Isotherms. The isotherm data for Xe and Kr in UTSA-74 at 273 and 298 K were fitted with the one-site Langmuir model

$$q = q_{sat}\frac{bp}{1 + bp}$$

with T-dependent parameters b

$$b = b_0 \exp\left(\frac{E}{RT}\right)$$

The Langmuir parameters are provided in Table 1.

Table 1. One-Site Langmuir Parameter Fits for Xe and Kr in UTSA-74

	q_{sat}, mol kg^{-1}	b_0, Pa^{-1}	E, kJ mol^{-1}
Xe	5.3	5.554×10^{-10}	24.4
Kr	7	1.266×10^{-09}	16.3

Isosteric Heat of Adsorption. The binding energy is reflected in the isosteric heat of adsorption Q_{st}, which is calculated based on the pure component equilibrium adsorption isotherms of Xe and Kr at 298 and 273 K through the equation as follows.

$$Q_{st} = RT^2\left(\frac{\partial \ln p}{\partial T}\right)_q$$

Ideal Adsorbed Solution Theory (IAST) Calculations. The adsorption selectivity for the Xe/Kr separation (20:80, v/v) is calculated based on the pure component equilibrium adsorption isotherms of Xe and Kr at 298 and 273 K through the equation as follows.

$$S_{ads} = \frac{q_1/q_2}{p_1/p_2}$$

Breakthrough Simulations. Transient breakthrough simulations were performed for 20/80 Xe/Kr mixtures in UTSA-74 operating at a total pressure of 100 kPa and 298 K, using the methodology described in earlier publications.[35] For the breakthrough simulations, the following parameter values were used: length of packed bed, L = 0.3 m; voidage of packed bed, τ = 0.4; superficial gas velocity at inlet, u = 0.04 m/s.

Grand Canonical Monte Carlo (GCMC) Simulations. The GCMC simulations, which were performed by Sorption code[36] in Material Studio (MS) software, were performed to investigate the adsorbed capacity of an MOF for Xe/Kr at 298 K from 0.001 to 100 kPa. A simulation box of 1 × 1 × 1 crystallographic unit cell was used. During the simulations, 4×10^6 steps were performed to guarantee the equilibration and to sample the desired properties, respectively. A rigid framework assumption was used in all the simulations. The universal force field (UFF)[37] was used to describe the interactions, and the van der Waals interaction with a cutoff of 12.5 Å was depicted by a Lennard-Jones 12−6 potential.

Density Functional Theory (DFT) Calculations. DFT calculations were performed to provide the optimized structures and energies for monomers, including USTA-74, Xe, and Kr. The Perdew−Burke−Ernzerhof (PBE) function under the generalized gradient approximation (GGA) functional with the double-ξ

https://dx.doi.org/10.1021/acs.inorgchem.0c01766
Inorg. Chem. 2020, 59, 11793−11800

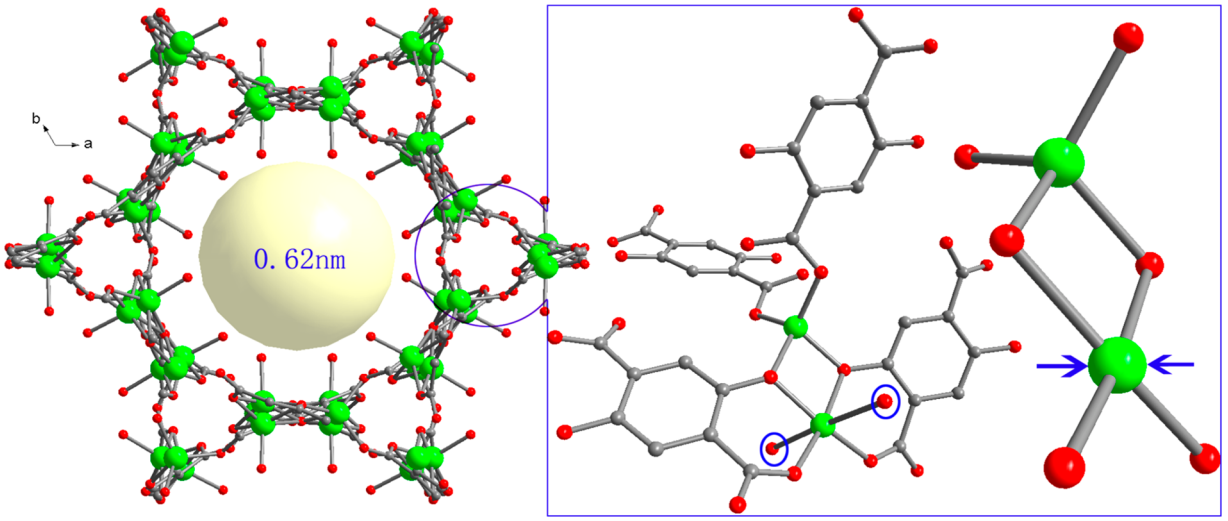

Figure 2. View of the structure of UTSA-74. This MOF shows a one-dimensional channel along the *c*-axis with pore size of 0.62 nm. The highlight is the coordination surrounding the metal ions. The circled atoms are terminal coordinated water molecules. The arrow presents the potential double-accessible open-metal site.

numerical polarization (DPN) basis set was used by the CASTEP program package[38] in the Materiel Studio of Accelrys. Because of the whole unit cell was too large to use, the smaller primitive cell was used. The tolerances of energy, gradient, and displacement convergence for optimizations were 1.0×10^{-5} eV/atom, 0.03 eV/Å, and 0.001 Å, respectively. The dispersion correction (DFT-D)[39] was considered in calculations of the single-point energy. The binding energy ΔE_{bind} for the adsorbed structures in the primitive cell with Xe/Kr was calculated based on the equation as follows

$$\Delta E_{bind} = \frac{1}{12}(E_{adsorbed} - 12E_{Xe/Kr} - E_{MOF})$$

where $E_{adsorbed}$, $E_{Xe/Kr}$, and E_{MOF} are the total energies of adsorbed structure, Xe/Kr gas, and a primitive cell of MOF, while the number 12 denotes that 12 Xe/Kr molecules can be adsorbed in one primitive cell.

RESULTS AND DISCUSSION

Structure of UTSA-74. The structure of UTSA-74 was reported by us recently.[35] It is an MOF-74 isomer, but it shows some distinct structural features (Figure 2). In UTSA-74, there are two crystallography-independent metal centers, showing two distinct coordination surroundings, one being the tetrahedral geometry finished by four oxygen atoms from organic ligands (thus without the potential as open-metal site) and one being the octahedral geometry finished by four oxygen atoms from organic ligands plus two terminal coordinated water molecules (accordingly with a potential double-accessible open-metal site). As estimated, UTSA-74 shows a higher density of open-metal site up to 8.25 mmol/cm^3 relative to MOF-74 with 7.5 mmol/cm^3. Also, on the basis of previous results, the activated samples indeed enable the unique structure of double-accessible open-metal site, suggesting its big potential for binding the Xe molecule.

Xe and Kr Adsorption in UTSA-74. Pure component equilibrium adsorption isotherms of Xe and Kr were measured at 298 and 273 K up to 1 bar, respectively (Figure 3). The total Xe uptake at 298 K and 1 bar was 2.71 mmol/g, whereas the Kr capacity under the same condition is just 0.58 mmol/g, giving a Xe/Kr ratio of 4.67. At 0.2 bar, the Xe/Kr uptake ratio is 6.5, while the Xe/Kr uptake ratio at 0.2 bar/0.8 bar is 1.89, which is comparable with the benchmark MOFs with an open-metal site such as Ni-MOF-74 (7.73, 2.18).[40] All these results imply selective adsorption of Xe in UTSA-74. A similar trend was observed at low temperature. At 273 K, the Xe capacity increases to 3.8 mmol/g, and the corresponding Kr uptake is 1.0 mmol/g. Accordingly, the Xe/Kr uptake ratio is 8.4 and 2.25 for 0.2 bar/0.2 and 0.2 bar/0.8 bar.

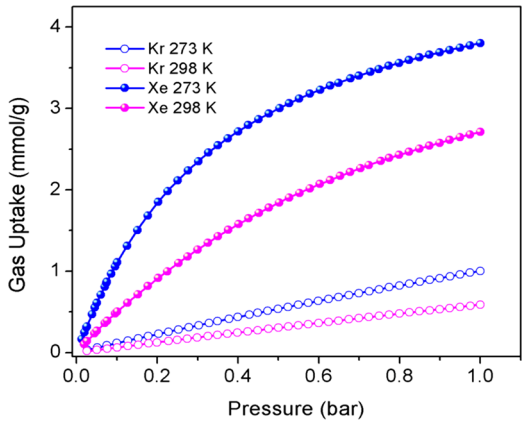

Figure 3. Xe and Kr adsorption isotherms at 298 and 273 K.

Xe/Kr Selectivity. The Xe/Kr selectivity was initially estimated by the generally used Henry's selectivity in light of the Xe and Kr adsorption data at low pressure.[33] At 298 K, the Henry's selectivity is 7.85, while it increases to 10.4 at 273 K. This Henry's selectivity is notably higher than that of previous MOFs with open-metal site such as Ni-MOF-74 (5.8),[7] MIL-101(Cr) (5.3),[21] MIL-101(Fe) (5.3),[21] and FMOF-Cu (1.4)[31] and comparable with the best-performing materials like those of $[Co_3(HCOO)_6]$ (8.7),[27] SB-MOF-2 (8.6),[28] and MOF-505 (6.8).[8] Then, we further performed the IAST calculation for a 20:80 (v/v) Xe/Kr mixture of gases at 298 K, giving the selectivity of 8.7−8.4 among the pressure arranged at 1−100 kPa (Figure 4), which is comparable with the Henry's selectivity and significantly higher than that of previous MOFs with an open-metal site such as Ni-MOF-74 (5−6),[7] Zn-MOF-74 (4−5),[7] Cu-BTC (2.6),[20] and FMOF-Cu (2.0)[31] and also comparable with the best-performing materials like those of $[Co_3(HCOO)_6]$ (12),[27] SB-MOF-2 (10),[28] and

https://dx.doi.org/10.1021/acs.inorgchem.0c01766
Inorg. Chem. 2020, 59, 11793−11800

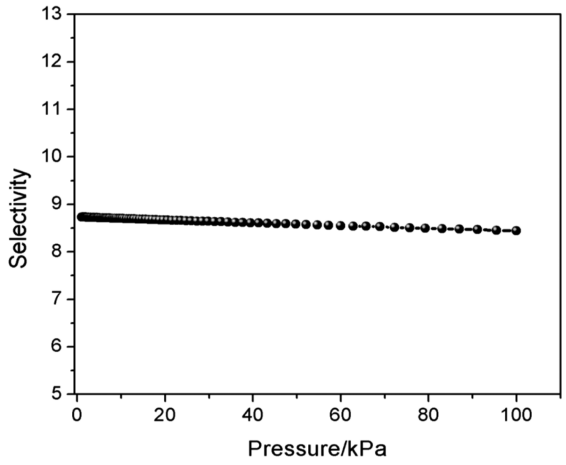

Figure 4. Xe/Kr selectivity of UTSA-74 for a 20:80 mixture of gases at 298 K.

MOF-505 (9−10).[8] Regarding the pore size of UTSA-74 being ∼1.0 nm, which is too large to match the Xe atom, all the above results suggest the open-metal site that is responsible for the selective Xe adsorption and stronger Xe-metal interactions in UTSA-74 over most reported MOFs with an open-metal site.

Isosteric Heats of Adsorption. To reflect the intensity of the interaction between the guest molecules and the MOF skeleton, the calculation of the isosteric heats of adsorption (Q_{st}) was performed (Figure 5). The Xe Q_{st} value at nearly zero loading is ∼24.4 kJ/mol, bigger than the corresponding value of 16.3 kJ/mol for Kr, implying a higher affinity for Xe over Kr and, consequently, selective adsorption of Xe. The isosteric heat of adsorption for Xe is bigger than that of the benchmark MOFs with open-metal site such as Ni-MOF-74 (22 kJ/mol),[40] also confirming stronger Xe-metal interactions in UTSA-74.

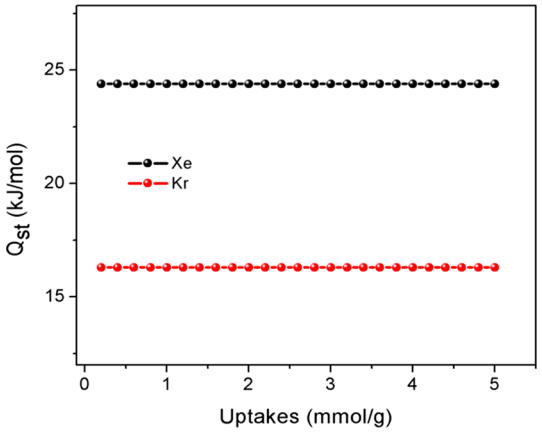

Figure 5. Q_{st} value of Xe and Kr for UTSA-74.

GCMC Simulation. To gain a better insight into the Xe and Kr adsorption in UTSA-74, a GCMC simulation was performed to explore the interactions between Xe/Kr and the MOF. According to the GCMC simulations for the Xe/Kr adsorption isotherm from 0.01−100 kPa and 298 K, the adsorption capacity of Xe (∼2.82 mmol/g) was found to be larger than that of Kr (0.59 mmol/g), which was well-consistent with the experimental results. At the same time, the density distribution of Xe/Kr can be obtained. The cases for Xe and Kr at 100 kPa were presented in Figure 6. Clearly, both Xe and Kr are mostly adsorbed around the open-metal site in UTSA-74.

To further disclose the binding ability and adsorption mechanism, DFT-D calculations were performed. The experimental crystal structure was slightly disordered on the open Zn site, so that the ordered geometry for UTSA-74 was built. The optimized structures of adsorption were acquired based on the density distribution of GCMC simulations. The binding energy of UTSA-74 with Xe was −31.35 kJ/mol, lower than the corresponding value of −17.96 kJ/mol for Kr, giving a 13.39 kJ/mol difference. This strongly suggests a preferred adsorption of Xe over Kr by UTSA-74. The calculated binding energy of Xe is comparable with the calculated value of −33.87 kJ/mol in Ni-MOF-74, which shows the highest calculated binding energy among all these MOF-74 series (Table 2).[41] In

Table 2. A Comparison of the Calculated Binding Energy of Xe and Kr with USTA-74 and MOF-74 Series

compounds	binding energy of Xe with metal (kJ/mol)	binding energy of Kr with metal (kJ/mol)
Zn-MOF-74	−22.87	−11.95
Co-MOF-74	−23.05	−13.34
Mg-MOF-74	−14.07	−4.53
Mn-MOF-74	−6.47	+3.44
Ni-MOF-74	−33.87	−23.61
UTSA-74	−31.35	−17.96

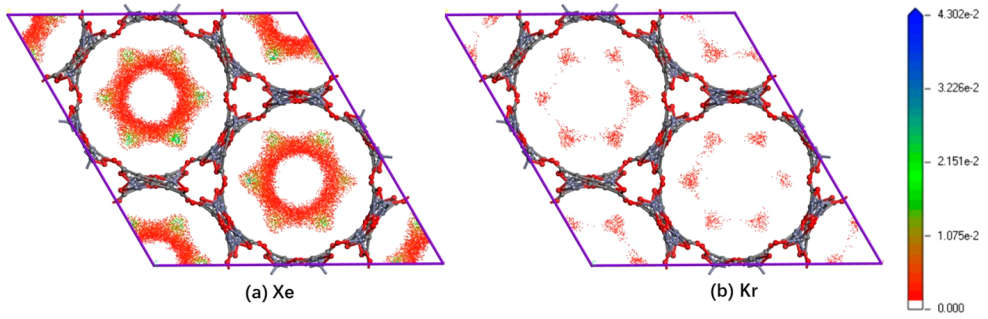

Figure 6. Simulated density distribution of Xe (a) and Kr (b) in UTSA-74 at 298 K and 100 kPa, where red = O, purple = Zn, while = H, gray = C, and the "color dots" denoted the size of density distribution.

https://dx.doi.org/10.1021/acs.inorgchem.0c01766
Inorg. Chem. 2020, 59, 11793−11800

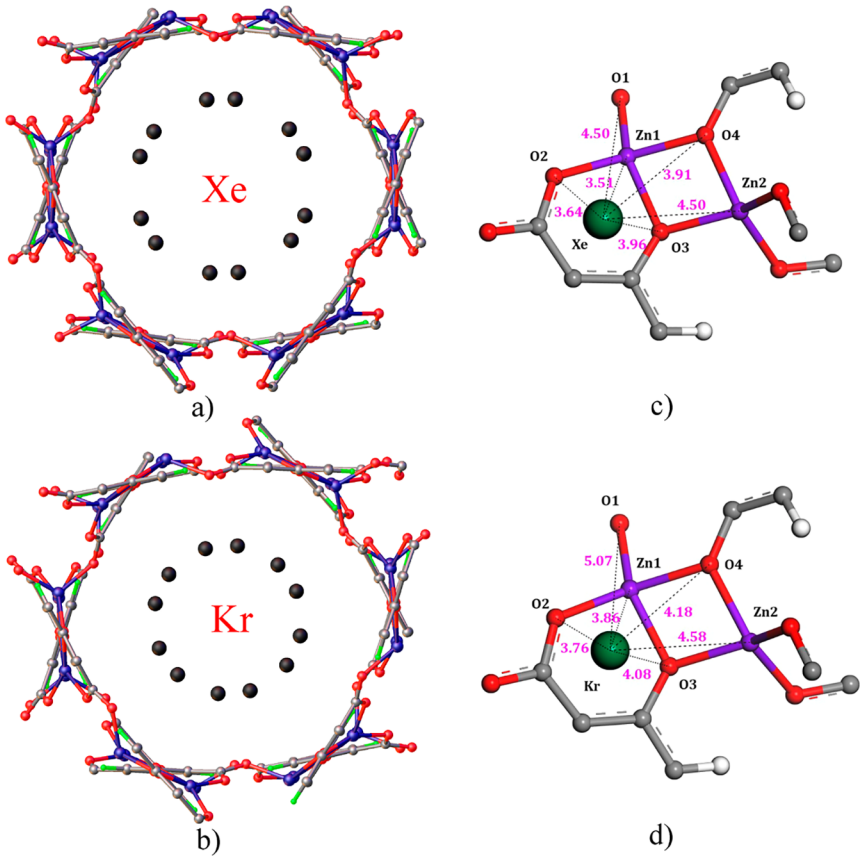

Figure 7. (a, b) View of the one-dimensional pore of USTA-74 with the occupation of Xe and Kr atoms. (c, d) View of the contact between Xe/Kr and other adjacent atoms, especially the open Zn site.

contrast to the single-open Zn site in Zn-MOF-74 with the calculated binding energy of −22.87 kJ/mol for Xe, the ultrahigh calculated binding energy up to −33.87 kJ/mol in our MOF should be derived from the unique double-open Zn site in this MOF. Furthermore, the shorter Xe−Zn distance of 3.5 Å than the Kr−Zn distance of 3.8 Å and the unique contact mode of two Xe or Kr atoms binding to one Zn via two open pathways was observed (Figure 7a−d). This clearly suggests stronger interactions between Xe and an open-metal site, which is well-consistent with the experimental results. On the basis of the above experimental and theoretical results, we made a conclusion that the selective adsorption mechanism in UTSA-74 is due to the unique double-open Zn site that preferentially provides two accessible pathways to binding with Xe atoms.

Transient Breakthrough Simulations. Transient breakthrough simulations[42−43] were performed for 20/80 Xe/Kr mixtures in UTSA-74 operating at a total pressure of 100 kPa and 298 K, using the methodology described in earlier publications. As shown in Figure 8, efficient separation was observed, where Kr breakthrough occurred first and after a certain time ($\Delta\tau$) Xe breakthrough was observed, mainly because of more efficient capture of Xe by the UTSA-74 bed.

Experimental Breakthrough. The experimental breakthrough test was implemented in a packed column of UTSA-74 to render the actual separation performance based on a 20:80 (v/v) Xe/Kr mixture of gases at 298 K under a total flow of 2 mL min^{-1}. As shown in Figure 9, it is clear that UTSA-74 can effectively separate the Xe/Kr mixture of gases, wherein Kr first eluted through the adsorption bed after 23 min, whereas Xe

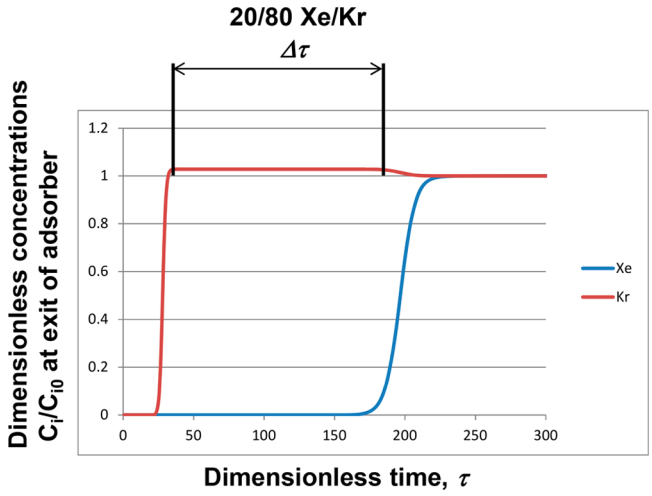

Figure 8. Plot of transient breakthrough simulations for UTSA-74.

breakthrough did not occur until 51 min. This suggests highly effective Xe/Kr separation by UTSA-74 materials. The Kr (>99.9%) production is 36 mL/g, and the Xe adsorption ability is 32 mL/g, slightly less than the value estimated from the Xe adsorption isotherm at 298 K. Most importantly, after a recycle test four times, no obvious decrease in the Xe/Kr separation performance was observed, confirming its good recyclability for the Xe/Kr separation.

https://dx.doi.org/10.1021/acs.inorgchem.0c01766
Inorg. Chem. 2020, 59, 11793−11800

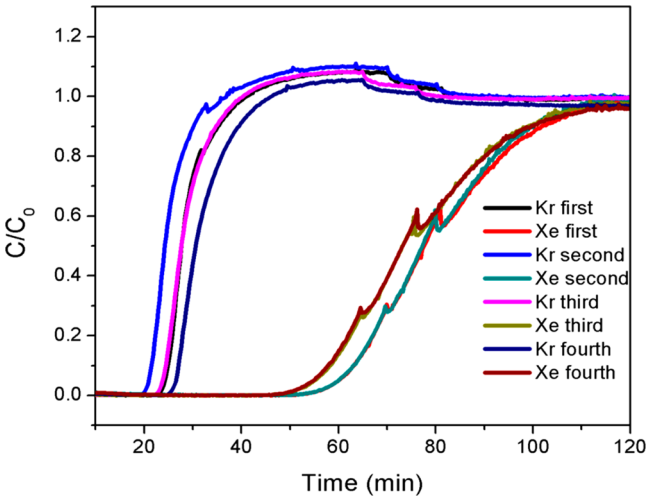

Figure 9. Experimental breakthrough plots based on a UTSA-74 bed at 298 K.

CONCLUSION

As discussed above, the MOF UTSA-74, due to the unique double-accessible open Zn site, even affords comparable binding ability with the single-open Ni site in Ni-MOF-74, as evidenced by the experimental Q_{st} value (24.4 kJ/mol for UTSA-74 vs 22 kJ/mol for Ni-MOF-74) and calculated Xe-metal binding energy (−31.35 kJ/mol for UTSA-74 vs −33.87 kJ/mol for Ni-MOF-74). For the MOF-74 series, Ni-MOF-74 (−33.87 kJ/mol) shows higher Xe-metal binding energy over all other MOF-74 derivatives such as Zn-MOF-74 (−22.87 kJ/mol), Mg-MOF-74 (−14.07 kJ/mol), and Co-MOF-74 (−23.05 kJ/mol).[41] In this regard, the category of metal ions will significantly affect the binding energy. Accordingly, the synthesis of Ni-based UTSA-74 derivatives with a unique double-accessible open Ni site is expected to show a higher Xe-metal binding ability and consequently a higher selective adsorption of Xe over Kr. And now we are working on this task.

Moreover, in contrast to the MOFs using a narrow pore to seriously restrict the Xe atoms, finally leading to a high selective adsorption of Xe over Kr, the available MOFs with open-metal site, whatever the single or double-accessible open-metal site, shows a bigger pore than the criterion for the Xe atom. This can be reflected on the experimental Q_{st} value. For example, our MOF shows the experimental Q_{st} value of 24.4 kJ/mol, far smaller than a rigid squarate-base MOF with perfect pore size (4.1 Å × 4.3 Å). Regarding the unique Xe-metal interactions observed in the MOFs with open-metal site, accordingly, it is proposed that constructing MOFs with both open-metal site and narrow pore size would be a good candidate to solve the Xe/Kr separation problem.

AUTHOR INFORMATION

Corresponding Author

Feng Luo − *State Key Laboratory of Nuclear Resources and Environment, School of Chemistry, Biology and Materials Science, East China University of Technology, Nanchang 330013, P. R. China;* orcid.org/0000-0001-6380-2754; Email: ecitluofeng@163.com

Authors

Yuan Tao − *State Key Laboratory of Nuclear Resources and Environment, School of Chemistry, Biology and Materials Science, East China University of Technology, Nanchang 330013, P. R. China*

Yaling Fan − *State Key Laboratory of Nuclear Resources and Environment, School of Chemistry, Biology and Materials Science, East China University of Technology, Nanchang 330013, P. R. China*

Zhenzhen Xu − *State Key Laboratory of Nuclear Resources and Environment, School of Chemistry, Biology and Materials Science, East China University of Technology, Nanchang 330013, P. R. China*

Xuefeng Feng − *State Key Laboratory of Nuclear Resources and Environment, School of Chemistry, Biology and Materials Science, East China University of Technology, Nanchang 330013, P. R. China*

Rajamani Krishna − *Van't Hoff Institute for Molecular Sciences, University of Amsterdam, Amsterdam 1098 XH, The Netherlands;* orcid.org/0000-0002-4784-8530

Complete contact information is available at: https://pubs.acs.org/10.1021/acs.inorgchem.0c01766

Author Contributions

F.L. conceived and designed the research; Y.T., Y.F., and X.F. performed the research; Z.X. performed the GCMC simulation and DFT-D calculation; R.K. performed the calculations of Q_{st}, IAST, and the transient breakthrough simulations.

Notes

The authors declare no competing financial interest.

ACKNOWLEDGMENTS

We thank the National Natural Science Foundations of China (21966002, 21871047), the Natural Science Foundation of Jiangxi Province of China (20181ACB20003), and the Training Program for Academic and Technical Leaders of Major Disciplines in Jiangxi Province (20194BCJ22010).

REFERENCES

(1) Lane, G. A.; Nahrwold, M. L.; Tait, A. R.; Taylor-busch, M.; Cohen, P. J.; Beaudoin, A. R. Anesthetics as teratogens: nitrous oxide is fetotoxic, xenon is not. *Science* **1980**, *210*, 899−901.

(2) Liu, L. T.; Xu, Y.; Tang, P. Mechanistic insights into xenon inhibition of NMDA receptors from MD simulations. *J. Phys. Chem. B* **2010**, *114*, 9010−9016.

(3) Kerry, F. G. *Industrial gas handbook: gas separation and purification;* CRC Press, 2007.

(4) Yang, R. T. *Gas separation by adsorption processes;* Butterworth-Heinemann, 2013.

(5) Liu, J.; Fernandez, C. A.; Martin, P. F.; Thallapally, P. K.; Strachan, D. M. A Two-column method for the separation of Kr and Xe from process off-gases. *Ind. Eng. Chem. Res.* **2014**, *53*, 12893−12899.

(6) Soelberg, N. R.; Garn, T. G.; Greenhalgh, M. R.; Law, J. D.; Jubin, R.; Strachan, D. M.; Thallapally, P. K. Radioactive iodine and krypton control for nuclear fuel reprocessing facilities. *Sci. Technol. Nucl. Install.* **2013**, *2013*, 1−12.

(7) Liu, J.; Thallapally, P. K.; Strachan, D. Metal-organic frameworks for removal of Xe and Kr from nuclear fuel reprocessing plants. *Langmuir* **2012**, *28*, 11584−11589.

(8) Ryan, P.; Farha, O. K.; Broadbelt, L. J.; Snurr, R. Q. Computational screening of metal-organic frameworks for xenon/krypton separation. *AIChE J.* **2011**, *57*, 1759−1766.

(9) Thallapally, P. K.; Grate, J. W.; Motkuri, R. K. Facile xenon capture and release at room temperature using a metal-organic framework: a comparison with activated charcoal. *Chem. Commun.* **2012**, *48*, 347−349.
(10) Gong, Y. J.; Tang, Y. M.; Mao, Z. H.; Wu, X. N.; Liu, Q.; Hu, S.; Xiong, S. S.; Wang, X. L. Metal-organic framework derived nanoporous carbons with highly selective adsorption and separation of xenon. *J. Mater. Chem. A* **2018**, *6*, 13696−13704.
(11) Li, J. L.; Huang, L.; Zou, X. Q.; Zheng, A. M.; Li, H. Y.; Rong, H. Z.; Zhu, G. S. Porous organic materials with ultra-small pores and sulfonic functionality for xenon capture with exceptional selectivity. *J. Mater. Chem. A* **2018**, *6*, 11163−11168.
(12) Cui, Y. J.; Li, B.; He, H. J.; Zhou, W.; Chen, B. L.; Qian, G. D. Metal-organic frameworks as platforms for functional materials. *Acc. Chem. Res.* **2016**, *49*, 483−493.
(13) Liao, P. Q.; Chen, H. Y.; Zhou, D. D.; Liu, S. Y.; He, C. T.; Rui, Z. B.; Ji, H. B.; Zhang, J. P.; Chen, X. M. Monodentate hydroxide as a super strong yet reversible active site for CO_2 capture from high-humidity flue gas. *Energy Environ. Sci.* **2015**, *8*, 1011−1016.
(14) (a) Li, B.; Wen, H. M.; Zhou, W.; Xu, J. Q.; Chen, B. L. Porous metal-organic frameworks: promising materials for methane storage. *Chem.* **2016**, *1*, 557−580. (b) Xu, Z. Z.; Xiong, X. H.; Xiong, J. B.; Krishna, R.; Li, L. B.; Fan, Y. L.; Luo, F.; Chen, B. L. A robust Th-azole framework for highly efficient purification of C_2H_4 from a $C_2H_4/C_2H_2/C_2H_6$ mixture. *Nat. Commun.* **2020**, *11*, 3163.
(15) Cui, X. L.; Chen, K. J.; Xing, H. B.; Yang, Q. W.; Krishna, R.; Bao, Z. B.; Wu, H.; Zhou, W.; Dong, X. L.; Han, Y.; Li, B.; Ren, Q. L.; Zaworotko, M. J.; Chen, B. L. Pore chemistry and size control in hybrid porous materials for acetylene capture from ethylene. *Science* **2016**, *353*, 141−144.
(16) Liao, P. Q.; Huang, N. Y.; Zhang, W. X.; Zhang, J. P.; Chen, X. M. Controlling guest conformation for efficient purification of butadiene. *Science* **2017**, *356*, 1193−1196.
(17) Wang, J.; Zhang, Y.; Zhang, P. X.; Hu, J. B.; Lin, R. B.; Deng, Q.; Zeng, Z. L.; Xing, H. B.; Deng, S. G.; Chen, B. L. Optimizing pore space for flexible-robust metal-organic framework to boost trace acetylene removal. *J. Am. Chem. Soc.* **2020**, *142*, 9744−9751.
(18) (a) Fan, W. D.; Yuan, S.; Wang, W. J.; Feng, L.; Liu, X.; Zhang, X. R.; Wang, X.; Kang, Z. X.; Dai, F. G.; Yuan, D. Q.; Sun, D. F.; Zhou, H. C. Optimizing multivariate metal-organic frameworks for efficient C_2H_2/CO_2 separation. *J. Am. Chem. Soc.* **2020**, *142*, 8728−8737. (b) Liu, R.; Liu, Q. Y.; Krishna, R.; Wang, W. J.; He, C. T.; Wang, Y. L. Water-stable europium 1,3,6,8-tetrakis(4-carboxylphenyl)pyrene framework for efficient C_2H_2/CO_2 separation. *Inorg. Chem.* **2019**, *58*, 5089−5095. (c) Wang, H. H.; Liu, Q. Y.; Li, L. B.; Krishna, R.; Wang, Y. L.; Peng, X. W.; He, C. T.; Lin, R. B.; Chen, B. L. Nickel-4′-(3,5-dicarboxyphenyl)-2,2′,6′,2″-terpyridine framework: efficient separation of ethylene from acetylene/ethylene mixtures with a high productivity. *Inorg. Chem.* **2018**, *57*, 9489−9494. (d) Zhang, P. D.; Wu, X. Q.; He, T.; Xie, L. H.; Chen, Q.; Li, J. R. Selective adsorption and separation of C_2 hydrocarbons in a "flexible-robust" metal-organic framework based on a guest-dependent gate-opening effect. *Chem. Commun.* **2020**, *56*, 5520−5523. (e) Wu, X. Q.; Xie, Y. B.; Liu, J. H.; He, T.; Zhang, Y. Z.; Yu, J. M.; Kong, X. J.; Li, J. R. Integrating multiple adsorption sites and tortuous diffusion paths into a metal-organic framework for C_3H_4/C_3H_6 separation. *J. Mater. Chem. A* **2019**, *7*, 25254−25257.
(19) Yu, M. H.; Space, B.; Franz, D.; Zhou, W.; He, C. H.; Li, L. B.; Krishna, R.; Chang, Z.; Li, W.; Hu, T. L.; Bu, X. H. Enhanced gas uptake in a microporous metal-organic framework via a sorbate induced-fit mechanism. *J. Am. Chem. Soc.* **2019**, *141*, 17703−17712.
(20) (a) Bae, Y.-S.; Hauser, B. G.; Colon, Y. J.; Hupp, J. T.; Farha, O. K.; Snurr, R. Q. High xenon/krypton selectivity in a metal-organic framework with small pores and strong adsorption sites. *Microporous Mesoporous Mater.* **2013**, *169*, 176−179. (b) Lee, S. J.; Yoon, T. U.; Kim, A. R.; Kim, S. Y.; Cho, K. H.; Hwang, Y. K.; Yeon, J. W.; Bae, Y. S. Adsorptive separation of xenon/krypton mixtures using a zirconium-based metal-organic framework with high hydrothermal and radioactive stabilities. *J. Hazard. Mater.* **2016**, *320*, 513−520.
(21) (a) Lee, S. J.; Kim, S.; Kim, E. J.; Kim, M.; Bae, Y. S. Adsorptive separation of xenon/krypton mixtures using ligand controls in a zirconium-based metal-organic framework. *Chem. Eng. J.* **2018**, *335*, 345−351. (b) Wang, T.; Peng, Y. L.; Lin, E.; Niu, Z.; Li, P. F.; Ma, S. Q.; Zhao, P.; Chen, Y.; Cheng, P.; Zhang, Z. J. Robust bimetallic ultramicroporous metal-organic framework for separation and purification of noble gases. *Inorg. Chem.* **2020**, *59*, 4868−4873.
(22) Gurdal, Y.; Keskin, S. Atomically detailed modeling of metal organic frameworks for adsorption, diffusion, and separation of noble gas mixtures. *Ind. Eng. Chem. Res.* **2012**, *51*, 7373−7382.
(23) Liu, J.; Strachan, D. M.; Thallapally, P. K. Enhanced noble gas adsorption in Ag@MOF-74Ni. *Chem. Commun.* **2014**, *50*, 466−468.
(24) Lee, S. J.; Kim, K. C.; Yoon, T. U.; Kim, M. B.; Bae, Y. S. Selective dynamic separation of Xe and Kr in Co-MOF-74 through strong binding strength between Xe atom and unsaturated Co^{2+} site. *Microporous Mesoporous Mater.* **2016**, *236*, 284−291.
(25) Wang, Y. L.; Liu, W.; Bai, Z. L.; Zheng, T.; Silver, M. A.; Li, Y. X.; Wang, Y. X.; Wang, X.; Diwu, J.; Chai, Z. F.; Wang, S. A. Employing an unsaturated Th^{4+} site in a porous thorium-organic framework for Kr/Xe uptake and separation. *Angew. Chem., Int. Ed.* **2018**, *57*, 5783−5787.
(26) Wang, H.; Yao, K. X.; Zhang, Z. J.; Jagiello, J.; Gong, Q. H.; Han, Y.; Li, J. The first example of commensurate adsorption of atomic gas in a MOF and effective separation of xenon from other noble gases. *Chem. Sci.* **2014**, *5*, 620−624.
(27) Chen, X. Y.; Plonka, A. M.; Banerjee, D.; Krishna, R.; Schaef, H. T.; Ghose, S.; Thallapally, P. K.; Parise, J. B. Direct observation of Xe and Kr adsorption in a Xe-selective microporous metal-organic framework. *J. Am. Chem. Soc.* **2015**, *137*, 7007−7010.
(28) Banerjee, D.; Simon, C. M.; Plonka, A. M.; Motkuri, R. K.; Liu, J.; Chen, X. Y.; Smit, B.; Parise, J. B.; Haranczyk, M.; Thallapally, P. K. Metal-organic framework with optimally selective xenon adsorption and separation. *Nat. Commun.* **2016**, *7*, 11831.
(29) Mohamed, M. H.; Elsaidi, S. K.; Pham, T.; Forrest, K. A.; Schaef, H. T.; Hogan, A.; Wojtas, L.; Xu, W. Q.; Space, B.; Zaworotko, M. J.; et al. Hybrid ultra-microporous materials for selective xenon adsorption and separation. *Angew. Chem., Int. Ed.* **2016**, *55*, 8285−8289.
(30) Fernandez, C. A.; Liu, J.; Thallapally, P. K.; Strachan, D. M. Switching Kr/Xe selectivity with temperature in a metal-organic framework. *J. Am. Chem. Soc.* **2012**, *134*, 9046−9049.
(31) Banerjee, D.; Cairns, A. J.; Liu, J.; Motkuri, R. K.; Nune, S. K.; Fernandez, C. A.; Krishna, R.; Strachan, D. M.; Thallapally, P. K. Potential of metal-organic frameworks for separation of xenon and krypton. *Acc. Chem. Res.* **2015**, *48*, 211−219.
(32) Li, L. Y.; Guo, L. D.; Zhang, Z. G.; Yang, Q. W.; Yang, Y. W.; Bao, Z. B.; Ren, Q. L.; Li, J. A robust squarate-based metal-organic framework demonstrates record-high affinity and selectivity for xenon over krypton. *J. Am. Chem. Soc.* **2019**, *141*, 9358−9364.
(33) Wang, Q. J.; Ke, T.; Yang, L. F.; Zhang, Z. Q.; Cui, X. L.; Bao, Z. B.; Ren, Q. L.; Yang, Q. W.; Xing, H. B. Separation of Xe from Kr with record selectivity and productivity in anion-pillared ultramicroporous materials by inverse size-sieving. *Angew. Chem., Int. Ed.* **2020**, *59*, 3423−3428.
(34) Luo, F.; Yan, C. S.; Dang, L. L.; Krishna, R.; Zhou, W.; Wu, H.; Dong, X. L.; Han, Y.; Hu, T. L.; O'Keeffe, M.; Wang, L. L.; Luo, M. B.; Lin, R. B.; Chen, B. L. UTSA-74: a MOF-74 isomer with two accessible binding sites per metal center for highly selective gas separation. *J. Am. Chem. Soc.* **2016**, *138*, 5678−5684.
(35) Allen, M. P.; Tildesley, D. J. *Computer simulation of liquids;* Clarendon Press: Oxford, UK, 1987.
(36) Rappé, A. K.; Casewit, C. J.; Colwell, K. S.; Goddard, W. A.; Skiff, W. M. UFF, a full periodic table force field for molecular mechanics and molecular dynamics simulations. *J. Am. Chem. Soc.* **1992**, *114*, 10024−10035.
(37) Clark, S. J.; Segall, M. D.; Pickard, C. J.; Hasnip, P. J.; Probert, M. I. J.; Refson, K.; Payne, M. C. First principles methods using CASTEP. *Z. Kristallogr. - Cryst. Mater.* **2005**, *220*, 567−570.

https://dx.doi.org/10.1021/acs.inorgchem.0c01766
Inorg. Chem. 2020, 59, 11793−11800

(38) Tkatchenko, A.; Scheffler, M. Accurate molecular van der waals interactions from ground-state electron density and free-atom reference data. *Phys. Rev. Lett.* **2009**, *102*, 073005.
(39) Perry, J. J.; Teich-mcgoldrick, S.; Meek, S. T.; Greathouse, J. A.; Haranczyk, M.; Allendorf, M. D. Noble gas adsorption in metal-organic frameworks containing open metal sites. *J. Phys. Chem. C* **2014**, *118*, 11685−11698.
(40) Vazhappilly, T.; Ghanty, T. K.; Jagatap, B. N. Computational modeling of adsorption of Xe and Kr in M-MOF-74 metal organic frameworks with different metal atoms. *J. Phys. Chem. C* **2016**, *120*, 10968−10974.
(41) Fan, C. B.; Le Gong, L.; Huang, L.; Luo, F.; Krishna, R.; Yi, X. F.; Zheng, A. M.; Zhang, L.; Pu, S. Z.; Feng, X. F.; Luo, M. B.; Guo, G. C. Significant enhancement of C_2H_2/C_2H_4 separation by a photochromic diarylethene unit: a temperature- and light- responsive separation switch. *Angew. Chem., Int. Ed.* **2017**, *56*, 7900−7906.
(42) Wu, H. Q.; Yan, C. S.; Luo, F.; Krishna, R. Beyond crystal engineering: significant enhancement of C_2H_2/CO_2 separation by constructing composite material. *Inorg. Chem.* **2018**, *57*, 3679−3682.

https://dx.doi.org/10.1021/acs.inorgchem.0c01766
Inorg. Chem. 2020, 59, 11793−11800